# Source Parameters of the Mw 6.6 Fandoqa (SE Iran) Earthquake of March 14, 1998

***Shobyr Ashkpour Motlagh[1] and Mehrdad Mostafazadeh[2]***

1. Ph.D. Student, Seismology Research Center, International Institute of Earthquake Engineering and Seismology (IIEES), Tehran, Iran, email: s.ashkpoor@iiees.ac.ir
2. Assistant Professor, Seismology Research Center, International Institute of Earthquake Engineering and Seismology (IIEES), Tehran, Iran

**ABSTRACT:** *In this study, the teleseismic body waveform modeling of the far-field P- and SH-waveforms as well as spectral analysis of P-waves are used to determine the source parameters of March 14, 1998 Fandoqa earthquake (Ms 6.9). Its epicenter is located southeast of Iran at Kerman province on the Gowk fault system. Previous focal mechanism solutions indicate motion on right-lateral strike slip faults. Based on waveform modeling, the results of this study represent a right-lateral strike slip motion on a NW-SE striking fault with parameters: Fault plane (strike=158°, dip=54° and the rake of 200°) and auxiliary plane (strike=58°, dip=76°, rake=-35°), depth of 4km and seismic moment of 1.32E+19N.m. The spectral analysis of the far-field P-wave pulses resulted in a fault length L ~ 20-26km, stress drop $\Delta\sigma$ ~ 23 bars and average displacement $\bar{u}$ ~ 1m. In this study, the variant models are also examined to determine the source dimension and it is found that both the Madariaga and Sato-Hirasawa models are more consistent with the surface faulting in this area.*

**Keywords:** Waveform modeling; Focal mechanism; Spectral analysis; Source dimension; Iran

## 1. Introduction

On March 14, 1998 at 19: 40: 28.3 *GMT* (23:10:28.3 Local time), a destructive earthquake of *Ms* 6.9 occurred in Kerman province of *SE* Iran on Gowk fault system, see Figure (1); epicenter of which was located at 30.138° *N*, 57.588° *E*. In this event with no foreshock, five people were killed in Golbaf, 50 were injured, 10000 become homeless, 2000 houses were destroyed, 1200 livestocks were killed and the utilities were disrupted. The event was felt at Baft and Kerman and damaged seven villages [Golbaf (*MMI* intensity *VII*), Zamanabad (*VII*), Fandoqa (*VII*), Hashtadan (*VII*), Jowshan (*VI*), Dehu (*VI*) and Deh Qanbar (*VI*)]. The main shock was followed by numerous aftershocks, the strongest of which ($m_b$ 4.9) occurred on March 27, 1998 at 16:20 *GMT*.

The events occurred on Gowk fault system since 1981, were mostly accompanied by coseismic surface ruptures, showing the shallow depths. This earthquake ruptured about 20*km* between Hasstedan in the north and Zamanabad in the south of Gowk fault system, a right-lateral strike-slip zone bordering the western edge of Dasht-e-Lut desert, and produced co-seismic faulting with horizontal offsets up to 3*m* [1]. Synthetic aperture radar (*SAR*) interferometry shows that a thrust, sub parallel to Gowk fault and projecting to the surface about 30*km* further east, also moved about 10*cm* in a time interval and location which makes it likely that its slip was triggered by the earthquake of March 14, 1998 [1]. The event is among the five earthquakes occurred on Gowk fault system, since 1981.

The aim of this paper is to investigate the source parameters of Fandoqa earthquake 14 March 1998 in detail. In this regard, a set of teleseismic data from Global Seismograph Network (*GSN*) was used. The focal mechanism and related parameters were determined using teleseismic waveform modeling [2]. Furthermore, the dimension of the average displacement across the ruptured area was determined from the far-field displacement spectra of the event.

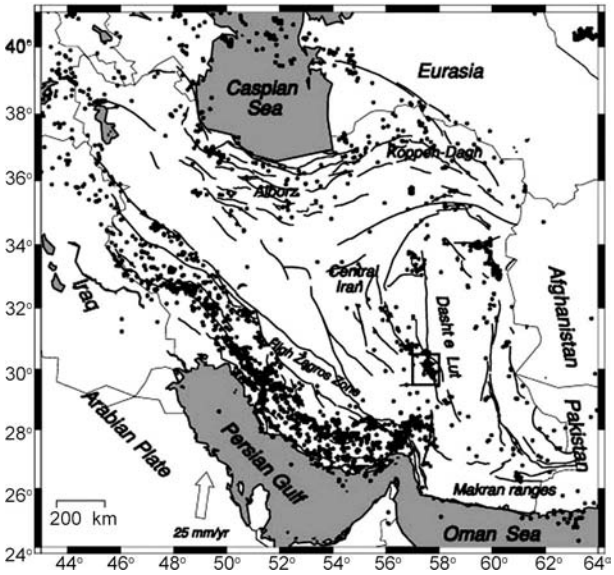


**Figure 1.** Iran map, showing the major fault zones and geographical regions. White arrow with 25mm/yr rate represents Arabia- Eurasia plate convergence [3]. Arabia- Eurasia convergence occurs in Zagros, Alborz, Kopeh Dagh, and possibly in central Iran by the rotation of strike-slip faults. Right lateral shear between central Iran and Afghanistan is taken up on N-S right -lateral faults of the Gowk-Nayband and Sistan suture zone systems, surrounding Dasht-e-Lut. The study area is marked by box. Dots show the distribution of instrumentaly recorded earthquake epicenters reported by Engdahl et al [4].

## 2. Tectonic Setting

Active tectonic of Iran is related to the convergence between Eurasia and Arabia plates, occurring at about $25mm.yr^{-1}$ at longitude $60^{o}E$ [3] and is mostly accommodated by distributed shortening within the political borders of Iran. About $10mm.yr^{-1}$ of Arabia-Eurasia convergence is accommodated in Zagros mountains in the *SW* of Iran [5-6], while the rest is mostly taken up in the seismic belts of the central Caspian, Alborz and Kopeh Dag of northern Iran, since central Iran itself is relatively flat, aseismic, and rigid. Whether shortening is not taken up in Zagros must be expressed as *N-S* right-lateral shear between central Iran and Afghanistan. This shear is manifested by major *N-S* right- lateral fault system on both west (in Kerman province) and east (in Sistan) sides of Dasht-e-Lut.

Kerman plateau is characterized by *NW-SE* to *N-S* trending ranges bounded by reverse and right- lateral strike-slip faults [5, 7, 8, 9]. Dasht-e-Lut desert is separated from Kerman plateau by the ranges on the southeast. Gowk fault system, marked by a narrow linear valley, cut these ranges in strike of $150^{o}$. The total length of fault system is about $160km$, from southern end of Nayband fault in the north to the Jebel Barez Mountains in the south. It turns *NW* and *SE* at its northern and southern ends, respectively where acquires apparently reverse components, see Figure (2).

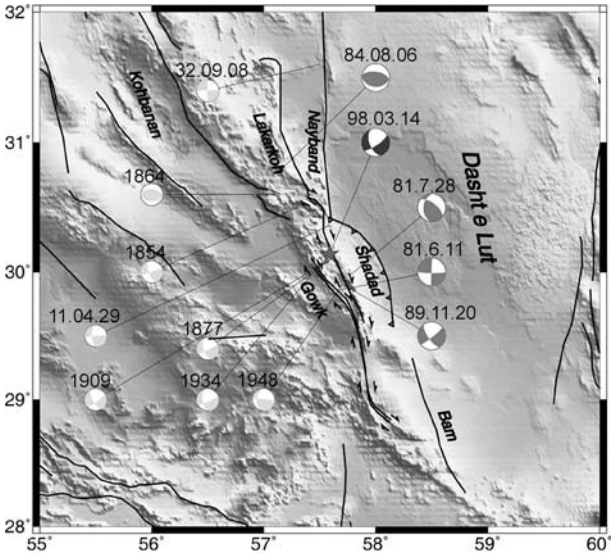


**Figure 2.** Tectonic map of Gowk area. The main faults are reported by IIEES. Beach balls show distribution and earthquake focal mechanisms of the events with Mw ≥ 5.5 which occurred in the study area. The mechanisms constrained by body wave inversion are in black (this study) and dark gray (HRV solutions). The light gray beach balls show the mechanisms of historical earthquakes which are estimated in this study.

## 3. Earthquakes

Gowk fault has been associated with five earthquakes of *Mw* = 5.4-7.1 in the past 26 years, see Figure (2) and Table (1). Other earthquakes of *Ms* = 5.6-6.2 in the region are known from historical records [10]. Although they seem usually difficult to be associated with particular faults, their focal mechanism are estimated based on well known faults and the earthquakes occurred recently in this region, see Figure (2).

All of them are smaller than the larger events of 1981 and 1998 and damaged the restricted areas relatively. Those that can plausibly be related to Gowk fault have their approximate damage regions marked on that assumption [1].

The March 14, 1998 Fandoqa earthquake (*Mw* = 6.6) ruptured $23km$ of the Gowk fault centered on Fandoqa, with an average right-lateral slip of ~$1.3m$ but with surface displacement up to $3m$ in places [11].

**Table 1.** Source parameters of Gowk region earthquakes. Epicenters, magnitudes (mb and Ms), and origin time are from Engdahl's [4]. Seismic moment ($M_0$) is in units of $10^{+18}$N.m. The last column gives the earthquake source parameters on each line: from body wave modeling in this paper (T1) Berberian [1], or USGS (U), and spectral analysis in this study (T2). Berberian [1] (B, B1 and B2 signify the first and second subevents in the June 11, 1981 earthquake) or from the CMT solutions by Harvard (H) or the USGS (U).

| Date | Time | Lat | Long | Depth | mb | Ms | Mw | Mo | Strike | Dip | Rake | R |
|---|---|---|---|---|---|---|---|---|---|---|---|---|
| 1981.06.11 | 07:24:24 | 29.86 | 57.68 | 20 | 6.1 | 6.7 | 6.58 | 4.18 | 169 | 52 | 156 | B1 |
| | | | | 12 | | | | 5.30 | 182 | 88 | 198 | B2 |
| | | | | 20 | | | 6.59 | 9.82 | 172 | 37 | 171 | H |
| | | | | 8 | | | 6.59 | 9.73 | 169 | 22 | 142 | U |
| 1981.07.28 | 17:22:24 | 29.99 | 57.79 | 18 | 5.7 | 7.1 | 6.98 | 36.69 | 177 | 69 | 184 | B |
| | | | | 15 | | | 7.24 | 90.10 | 150 | 13 | 119 | H |
| | | | | 22 | | | 7.02 | 43.20 | 293 | 67 | 115 | U |
| 1989.11.20 | 04:19:07 | 29.90 | 57.72 | 10 | 5.6 | 5.5 | 5.83 | 0.70 | 145 | 69 | 188 | B |
| | | | | | | | 5.88 | 0.82 | 148 | 81 | 165 | H |
| **1998.03.14** | **19:40:28** | **30.138** | **57.588** | **4** | **5.9** | **6.9** | **6.6** | **13.19** | **158** | **54** | **200** | **T1** |
| | | | | | | | | **8.94** | | | | **T2** |
| | | | | 5 | | | 6.57 | 9.09 | 156 | 54 | 195 | B |
| | | | | 15 | | | 6.58 | 9.43 | 154 | 57 | 186 | H |
| | | | | 8 | | | 6.52 | 7.70 | 146 | 58 | 181 | U |
| 1998.11.18 | 07:39:27 | 30.32 | 57.53 | 15 | 4.9 | 5.1 | 5.34 | 0.13 | 174 | 55 | 173 | H |

## 4. Teleseismic Waveform Modeling

### *4.1. Methodology and Application*

The technique of body-waveform modeling, fully described by Nabelek [2] and McCaffery et al [12] is used to calculate the focal mechanism of Fandoqa earthquake. The applied data, consist of *P* and *SH* waveforms, are from Global Seismograph Network (*GSN*) stations. All waveforms had the sampling frequency of 1*Hz* and were recorded at epicentral distances ranges of $30^o$ to $90^o$ as teleseismic distance. At teleseismic distance P- and S-waves arrive quite separately (in time) from each other, as well as other seismic phases and therefore, they can be analyzed independently. The wave forming packets of teleseismic P- and S-waves are characterized by essentially constant ray parameters and involved all direct, reflected, and converted waves which propagated through the earth's mantle along the path of minimum travel times.

The *MT*5 version [13] of McCaffery and Abers [14] algorithm were used to invert *P* and *SH* waveform data and to obtain the strike, dip, rake, centroid depth, seismic moment, and source time function of the examined event. The methodology assumes that the source (with *Ms* ~6.6) can be represented as a point source (the centroid) in space, although not in time. The time history of the displacement on the fault was represented by a source time function making a series of overlapping isosceles triangles, the numbers and duration of which were defined by the user. The inversion routine yield amplitudes were corrected for each triangular shape. Amplitudes were corrected for the geometrical spreading, the epicentral distance [15], and the attenuation using Futterman's [16] operator with $t^* = 1s$ for *P*- and $t^* = 4s$ for *SH*-waves. The inversion adjusts the relative amplitudes of the source time function elements, the centroid depth, the seismic moment, and the source orientation (strike, dip, and rake) to minimize the misfit between observed and synthetic seismograms. We refer to this solution as the minimum misfit solution. The covariance matrix associated with the minimum misfit solution usually underestimates the true uncertainties associated with the source parameters. In order to find more realistic uncertainties, the methodology of McCaffery and Nabelek [17] and Molnar and Lyon-Caen were followed [18] by fixing some of the source parameters at values close to, but different from those of the minimum misfit solution and allowing all other parameters to vary during the inversion. The errors are determined by visual examination when the match of the observed to synthetic seismograms significantly deteriorates. Synthetics were generated for a point source buried in a half-space.

### *4.2. Inversion Results*

The focal mechanism of March 14, 1998 earthquake was computed by inverting 26 *P*-and 15 *SH*- Long-Period waves with good azimuthally coverage, see Figure (3). The results are shown in Figures (4) and

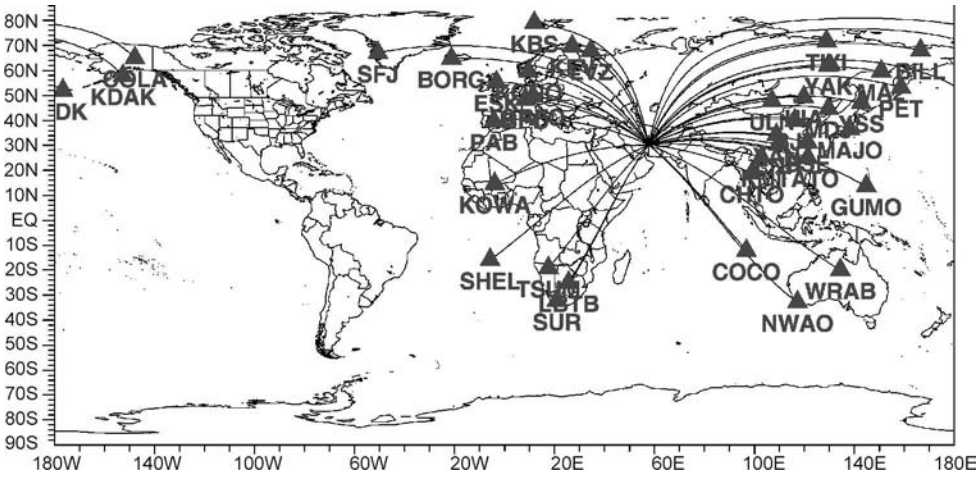


**Figure 3.** Map of Incorporated Research Institutions for Seismology (IRIS) stations ($\Delta$ =30°-90°) which their seismograms are used in this study, show the appropriate azimuthally distribution. The triangles show the location of the stations, and alphabetic marks illustrate the station codes.

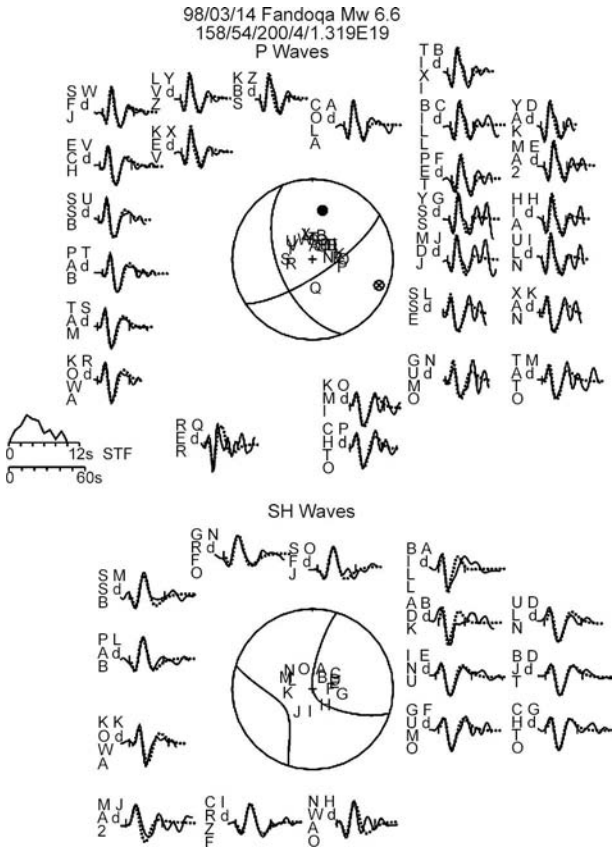


**Figure 4.** Minimum misfit solution for the 14 March 1998 earthquake in Gowk fault, see Table (2), showing P (top) and SH (bottom) observed (solid) and synthetic (doted) waveforms. Waveforms for each station are arranged azimuthally around the focal spheres. Station positions on focal spheres are identified by capital letters and arranged clockwise starting from north. STF is the source time function. Vertical ticks on the seismograms indicate the inversion window. Numbers beneath the header line are strike, dip, rake, centroid depth (km) and scalar moment (N.M). Stations were weighted according to azimuthally density and then S seismograms weights were halved to compensate for their larger amplitudes. P and T axes are represented by a black and white dot.

(5) and Table (1). The solution indicates right lateral strike-slip on a fault dipping 54° (±5°) *SW*, with a strike of 158° (-10°/+11°), a rake of 200° (-11°/+9°) a hypocentral depth of 4*km* (±2), and a source time function with a duration of 10 seconds while the 95% of the energy was abruptly released within first 9*sec*., and a scalar moment of 1.319 E+19*N.m.* All inversions were carried on a supposed half space with $Vp = 6.5 km.s^{-1}$, $Vs = 3.7 km.s^{-1}$, and $\rho = 2.85 gr.cm^{-3}$. Our solution is in good agreement with the records published in the Harvard *CMT* catalogue and Berberian et al [1], except in seismic moment in which our result indicates a larger value than those obtained in previous studies, see Table (1), and we think it is more consistent with the observed average displacement.

## 5. Source Parameters from Far-Field Displacement Spectra

### *5.1. Methodology*

Source parameters such as seismic moment ($M_o$), fault length ($L$), average displacement ($\bar{u}$) across the fault and static stress drop ($D\sigma$), were determined for the Fandoqa mainshock, using the far-field amplitude displacement spectra. The data consist of long period P-waves with sampling frequency of 1*Hz* which was recorded at teleseismic distances (30°-90°) from the *GSN* stations. In order to include amplitudes comparable to the maximum amplitudes of the P-wave train, a time window was used starting at the P- arrival and ending before the S-wave arrival and therefore contained both P-wave and its coda. The displacement waveform was corrected for the

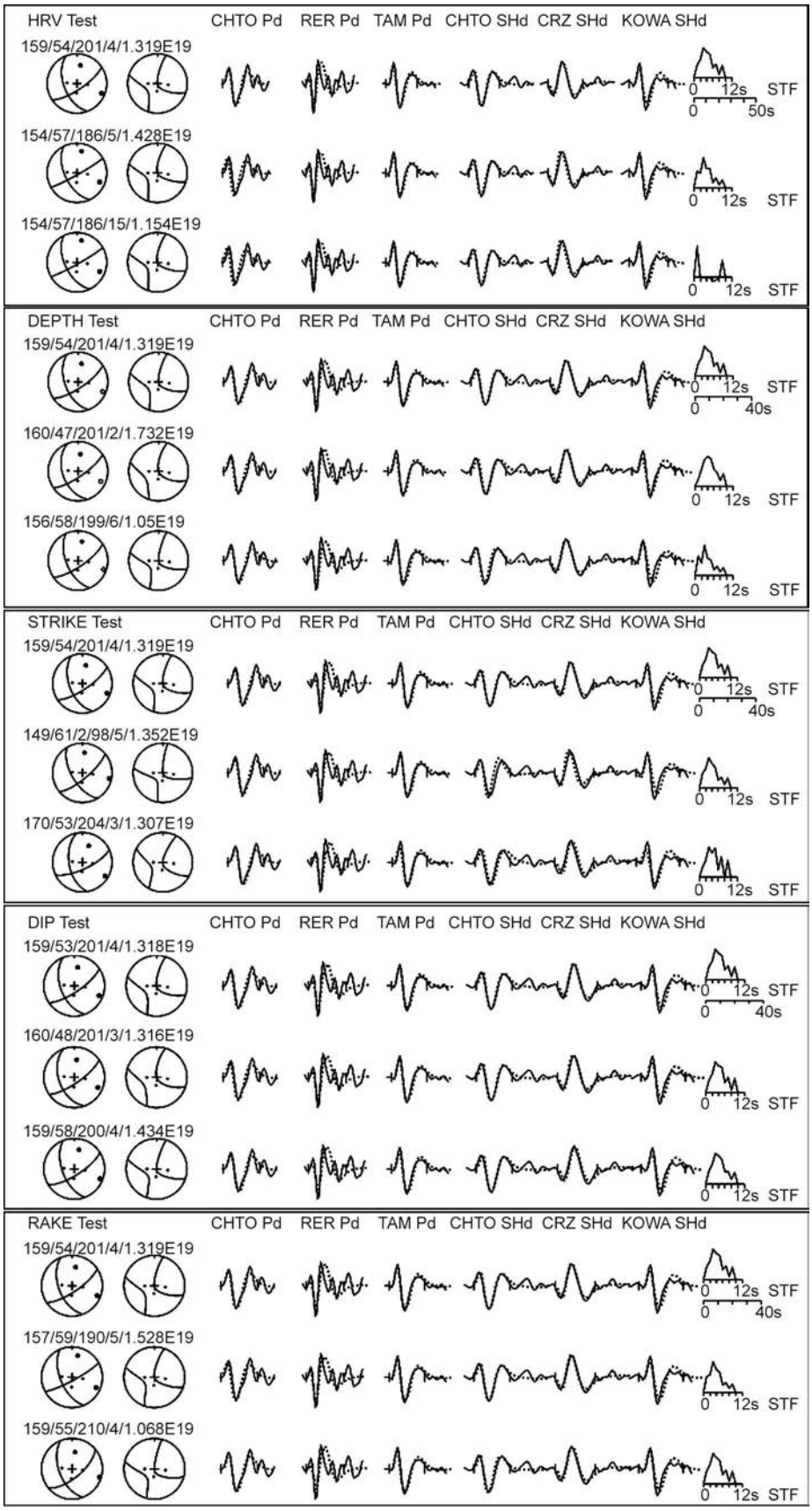


**Figure 5.** Tests to check the inversion for Mach 14, 1998 earthquake, see Figure (4), for sensitivity source parameters. Synthetic seismograms are dotted and the observed are solid lines. The first line in each shows the minimum misfit solution from Figure (4). P and SH focal spheres are shown, with the time function and numbers showing the strike, dip, rake, centroid depth and seismic moment. First box shows the HRV CMT tests, first line in this box indicates the best fit in this study, second line is the HRV solutions with all parameters fixed, and the last line shows the CMT solutions depth free. We carried out the velocity structure in this study, a half space of Vp = 6.5km.s$^{-1}$, Vs =3.7km.s$^{-1}$, and ρ =2.85g.cm$^{-3}$, respectively. The boxes show the depth, strike, dip, and rake tests.

instrument response, attenuation and radiation pattern. The far-field amplitude displacement spectra were characterized by 3 parameters: i) the low frequency level $W_o$, which is proportional to seismic moment; ii) the corner frequency, $f_c$, and iii) the power of the high frequency asymptote. Following Brune [19-20], the corner frequency at the intersection of low-and high-frequency asymptotes in the spectrum was defined.

Almost all far-field displacement spectra were characterized by a constant low-frequency level, $W_o$, and a fall-off above a corner frequency $f_c$, at a rate proportional to $f^y$. Spectra that did not show such a shape was not analyzed. Determination of the spectral parameters ($W_o$, $f_c$) was performed by eye fitting low- and high-frequency asymptotes to the observed spectra. Figure (6) shows indicatively the displacement amplitude spectra for 6 stations together with their best fitting results.

The scalar seismic moment was calculated from

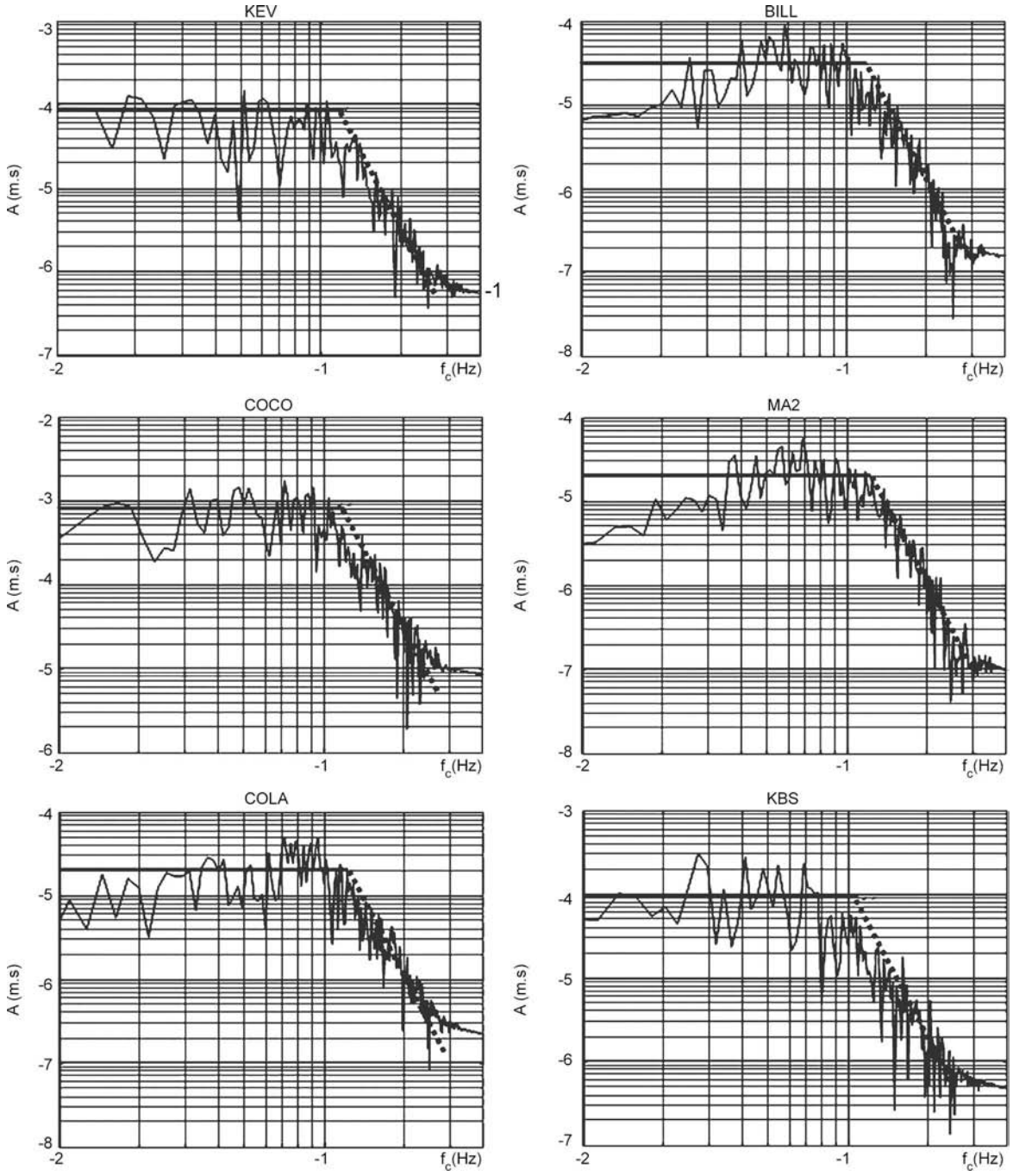


**Figure 6.** Far-field amplitude displacement spectra was used to estimate the fault dimensions and other parameters of the Fandoqa mainshock. The low and high frequency asymptotes (fitted by eye) are depicted as straight lines. The corresponding values of the low-frequency part of the spectrum, $\Omega_o$, and the corner frequency, $f_c$, are also shown for each spectrum.

the relation [21]:

$$M_o(P) = 4\pi\rho R\alpha^3\left[W_o(P)/R_{\theta\varphi}\right] \quad (1)$$

where $W_o(P)$ denotes the low-frequency asymptote of the spectrum, $\rho$ shows the density at the source, $R_{\theta\varphi}$ as the radiation pattern coefficient for P-waves from a double couple point source, $R$ is the epicentral distance and $\alpha$, is the P-wave velocity at the source.

In order to calculate the source dimensions and the stress drop, a circular fault of radius $r$ was assumed. To estimate the fault radius, four models were examined as follows:

$$r(P) = 0.32\beta / f_{cp} \quad \text{Madariaga Model [22]} \quad (2)$$

$$r(P) = 0.37\alpha / f_{cp} \quad \text{Brune Model [20]} \quad (3)$$

$$r(P) = 0.24\alpha / f_{cp} \quad \text{Sato and Hirasawa Model [23]} \quad (4)$$

$$r(P) = 0.10\beta / f_{cp} \quad \text{Bresnev Model [24]} \quad (5)$$

where $f_{cp}$ is the corner frequency of the P-wave spectra and $\beta$ is the velocity of shear waves. It is also assumed that the diameter of the circular fault area is equal to the observed fault length [25].

Stress drop was calculated from the relation of Keilis-Borok [21]:

$$D\sigma = (7M_o)/16r^3 \quad (6)$$

and the average displacement, $\bar{u}$, was calculated from the relation of Aki [26]:

$$M_o = \mu A\bar{u} \quad (7)$$

where $\mu$ is the shear modulus (taken equal to $3\times10^{10} N.m^{-2}$) and $A$ is the fault surface.

Average values <$x$> were computed for each parameter (stress drop, fault length, average displacement) following Archuleta et al [27]:

$$< x > = \text{anti}\, Log\left[(1/N)\sum log\, x_i\right] \quad (8)$$

where $N$ is the number of stations used. The basic reason for using this relation is that in the case of simple arithmetic average, the mean values are biased towards the larger values. The corresponding standard deviation of the logarithm $SD$ ($log$ <$x$>) and the multiplicative error factor, $E_x$, were also calculated from the relations of Archuleta et al [27]:

$$SD(Log < x >) = \left[\frac{1}{N-1}\sum (\text{Log}x_i - \text{Log} < x >)^2\right]^{1/2} \quad (9)$$

$$E_x = \text{anti Log}\left(SD\,(\text{Log} < x >)\right) \quad (10)$$

### 5.2. Source Parameters from the Spectral Analysis

For all calculations, values of $6.5 km.s^{-1}$ and $3.7 km.s^{-1}$ for the P- and S-waves velocity, were used respectively, as well as a density of $2.85 g.cm^{-3}$, and a value of $3\times10^{10}$ for the shear modulus, $\mu$.

The distance, the azimuth, the low frequency asymptote, $W_o$ and the corner frequency ($f_c$) of 33 stations that were used are listed in Table (2). Table (3) lists the average values and the multiplicative factor of the average of scalar seismic moment ($M_o$), average radius ($r$) or the half length of the fault, the stress drop ($\Delta\sigma$), and the average displacement across the fault, for a circular fault model.

**Table 2.** Station and spectral parameters obtained from far-field displacement spectra of P-waves for March 14, 1998 Fandoqa earthquake. Columns shows the station code, station azimuth, take-off angle, station distance from earthquake epicenter, low-frequency asymptotes of spectrum, and corner frequency, respectively.

| S-Code | Az (deg) | Ta (deg) | Dis (km) | $W_o$ (m.s) | $f_c$ (Hz) |
|---|---|---|---|---|---|
| CHTO | 97.1 | 29.2 | 4350 | 3.8E-5 | 0.11 |
| KMI | 85.9 | 28.9 | 4459 | 1.2E-4 | 0.09 |
| LVZ | 374 | 28.9 | 4464 | 6.1E-5 | 0.11 |
| BFO | 310 | 28.2 | 4611 | 2.2E-5 | 0.087 |
| KEV | 345 | 28.4 | 4812 | 8.9E-5 | 0.92 |
| XAN | 71 | 28.4 | 4813 | 1.8E-4 | 0.10 |
| KONO | 328 | 28 | 4842 | 5.5E-5 | 0.10 |
| ENH | 76.2 | 27.6 | 4948 | 2.6E-4 | 0.092 |
| BJT | 61.6 | 27.1 | 5355 | 1.9E-4 | 0.09 |
| HIA | 49.1 | 26.6 | 5500 | 1.8E-5 | 0.10 |
| ESK | 319 | 26.3 | 5587 | 6.9E-4 | 0.11 |
| PAB | 298 | 26.2 | 5650 | 8.8e-5 | 0.10 |
| KBS | 350 | 25.9 | 5849 | 9.0E-5 | 0.10 |
| SSE | 71.7 | 25.5 | 6007 | 3.1E-5 | 0.11 |
| YAK | 33 | 25 | 6171 | 1.1E-5 | 0.092 |
| TIXI | 21.3 | 24.9 | 6204 | 4.1E-5 | 0.11 |
| TATO | 78.6 | 24.4 | 6253 | 5.0E-5 | 0.11 |
| COCO | 132.2 | 24.3 | 6289 | 6.8E-4 | 0.11 |
| MDJ | 53.9 | 24.2 | 6365 | 5.0E-5 | 0.09 |
| KOWA | 269 | 23.7 | 6500 | 1.1E-4 | 0.10 |
| BORG | 330 | 24.1 | 6503 | 3.82E-5 | 0.16 |
| TSUM | 223.3 | 22.9 | 7150 | 1.8E-5 | 0.14 |
| LBTB | 212.7 | 22.4 | 7200 | 2.85E-5 | 0.12 |
| YSS | 48.6 | 22 | 7287 | 3.90E-5 | 0.11 |
| MA2 | 33.8 | 22 | 7345 | 2.0E-5 | 0.12 |
| BILL | 22.4 | 20.8 | 7675 | 3.10E-5 | 0.11 |
| SFJ | 336.5 | 21 | 7708 | 3.0E-5 | 0.13 |
| SUR | 212.3 | 20.3 | 7929 | 2.40E-4 | 0.14 |
| PET | 38.4 | 20.1 | 8079 | 1.20E-5 | 0.13 |
| SHEL | 201 | 19.8 | 8482 | 2.0E-4 | 0.15 |
| COLA | 10.6 | 17.4 | 9254 | 1.20E-5 | 0.12 |
| NWAO | 133.2 | 17.1 | 9368 | 2.70E-5 | 0.11 |
| WRAB | 113.7 | 16.1 | 9897 | 3.92E-4 | 0.10 |

**Table 3.** Mean values and multiplicative error factors of the seismic moment, $M_o$, the fault radius, which are obtained from Brune model [19-20] $r_B$, Madariaga model [22] $r_M$, Sato and Hirasawa model [23] $r_S$, and Bresnev model [24] $r_{Br}$, the stress drop, $\Delta\sigma$ and the average displacement, $\bar{u}$ , as defined by means of the far-field P-waves spectral analysis.

| | $M_o$ $(N.m)$ | $r_B$ $(km)$ | $r_M$ $(km)$ | $r_S$ $(km)$ | $r_{Br}$ $(km)$ | $\Delta\sigma$ $(bar)$ | $\bar{u}$ $(m)$ |
|---|---|---|---|---|---|---|---|
| Average Value | 8.89E+18 | 20.56 | 10.12 | 13.34 | 3.16 | 23.4 | 0.955 |
| Errors | 2.944E+18 | ±1.5 | ±1.5 | ±1.5 | ±1.5 | ±4.8 | ±0.32 |

The value of the scalar seismic moment based on relation (1), is $8.894\times10^{18}N.m$, which is approximately comparable to one obtained from body waveform modeling by previous studies.

By comparing results of the four models, large differences were observed between them. For example, the Brune circular model results in a fault length of ~44$km$ (2$r$), considerably overestimated, and the Bresnev circular model results in a length of ~7$km$ which is underestimated as compared to other models. It seems that the reliable result for the fault length in this event is based on the Madariaga model which is in good agreement with one obtained from surface rupture [1].

## 6. Discussion and Conclusions

We investigated the source parameters of the Fandoqa *Ms* 6.9 earthquake that occurred in the southeast Iran at Kerman province using body waveform modeling and the spectral analysis of the far-field displacement P-wave spectra. To ensure a reliable estimation of the scalar seismic moment, the waveform modeling and far-field spectral analysis were used in parallel.

The parameters of the March 14, 1998 Fandoqa earthquake, averaging the values obtained, are: fault plane (strike = 158°, dip = 54°, rake = 200°) and auxiliary plane (strike = 58°, dip = 76°, rake = -35°), depth 4$km$, and $M_o = 1.32\times10^{19}N.m$, fault length $L$~ 20$km$ which is in good agreement with that obtained based on surface faulting, stress drop $\Delta\sigma$~ 23 bars and average displacement $\bar{u}$ ~ 95.5$cm$.

In order to determine the fault dimension, the various circular models were tested and it was found that the Madariaga Model [21] is in more agreement with comparison to observed values.

Figures (4) and (5) show the focal mechanism and parameter tests of the Fandoqa earthquake.

It seems that the *NW-SE* striking plane is the fault plane which implies sinisteral strike-slip motion contrary to what is expected from the strands of the Gowk fault zone which terminates in this area, and is well known for its activities. The results show the seismic moment value that is larger than those obtained in previous studies, and because of the observed average displacement, we think our result is more consistent.

Although the spectral P-wave analysis results is used in a reliable fault dimension, it is certainly difficult to obtain the seismic moment values. The spectral analysis shows that both the Madariaga [22] and Sato-Hirasawa [23] models are more consistent to determine the fault dimensions in Gowk fault systems in comparison to other models.

## Acknowledgement

This work is related to Ph.D. project (5323 code) of the first author at International Institute of Engineering Earthquake and Seismology (*IIEES*). We would like to thank the *IRIS* team for providing data as well as the Harvard University for providing the *CMT* solutions. We thank Professor Engdahl who kindly provided us with the final catalogue of events in Iran. Special thanks is also extended to Professor James Jackson, Dr. Keith Priestley, Dr. Alessia Maggi, and Dr. Peter Zwick for their constructive comments during the course of this research. We are grateful to Dr. Yasamin Izadkhah for proofreading the paper.

## References

1. Berberian, M., Baker, C., Fieling, E., Jackson, J.A., Parsons, B.E., Priestley, K., Qorashi, M. Talebian, M., Walker, R., and Wright, T. J. (2001). "The March 14, 1998 Fandoqa Earthquake (Mw 6>6) in Kerman Province, SE Iran: Re-Rupture of the 1981 Sirch Earthquake Fault, Triggering of Slip on Adjacent Thrusts, and the Active Tectonics of the Gowk Fault Zone", *Geophysical Journal International*, **146**, 371-398.

2. Nabelek, J. (1984). "Determination of Earthquake Source Parameters from Inversion of Body Waves", PhD Thesis, Massachusetts Institute of Technology.

3. Vernant, P., Nilforoshan, F., Hatzfeld, D. et al (2004a). "Present-Day Crustal Deformation and Plate Kinematics in Middle East Constrained by GPS Measurements in Iran and Northern Oman", *Geophys. Journal Int.*, **157**, 381-398.

4. Engdahl, E.R., Van Der Hilst, R., and Buland, R. (1998). "Global Teleseismic Earthquake Relocation with Improved Travel Time and Procedures for Depth Determinations", Bull. Seismol. Soc. Am., **98**, 722-743.

5. Tatar, M., Hatzfeld, D., Martinod, J., Walpersdorf, A., Ghafory-Ashtiany, M., and Chery, J. (2002). "The Present-Day Deformation of Central Zagros from GPS Measurements", *Geophys, Res. Lett.*, **29**(19), 1927, doi: 10.1029/2002GL015427.

6. Hessami, K. (2002). "Tectonic History and Present-Day Deformation in the Zagros Fold-Thrust Belt", Ph.D. Thesis, Univ. of Uppsala, Sweden.

7. Berberian, M. (1981). "Active Faulting and Tectonics of Iran, in Zagros, Hindu Kush, Himalia: Geodynamic Evolution", Geodyn. Ser., **3**, edited by Gupta, H.K. and Delany, F.M., 33-69, AGU, Washington, D.C.

8. Jackson, J. and McKenzie, D. (1984). "Active Tectonics of the Alpine-Himalayan Belt between Turkey and Pakistan", *Geophys. Journal R. Astron. Soc.*, **77**, 185-264.

9. Berberian, M., and Yeats, R.S. (1999). "Patterns of Historical Earthquake Rupture in the Iranian Plateau", Bull. Seismol. Soc. Am., **89**, 120-139.

10. Ambraseys, N.N. and Melville, C.P. (1982). "A History of Persian Earthquakes", Cambridge University Press, London, 219p.

11. Walker, R. and Jackson., J. (2002). "Offset and Evolution of the Gowk Fault, S.E. Iran: A Major Intra-Continental Strike-Slip System", *Journal of Structural Geology*, **24**, 1677-1698.

12. McCaffery, R., Zwick, P., and Abers, G. (1991). "SYN 4 Program", IASPEI Software Library, **3**, 81-166.

13. Zwick, P., McCaffery, R., and Abers, G. (1994). "MT5 Program", IASPIE Software Library, 4.

14. McCaffery, R. and Abers, G. (1988). "SYN3: A Program for Inversion of Teleseismic Body Waveforms on Microcomputers", Air Force Geophys. Lab. Tech. Report, AFGL-TR-88-0099, Hanscomb Air Force Base, Ma.

15. Langston, C. and Helmberger, D.V. (1975). "A Procedure for Modeling Shallow Dislocation Sources", *Geophysics. Journal R. Astorn. Soc.*, **42**, 117-130.

16. Futterman, W. (1962). "Dispersive Body Waves", *Journal Geophys. Res.*, **67**, 5279-5291.

17. McCaffery, R. and Nabelek, J. (1987). "Earthquakes, Gravity and the Origin of the Bali Basin: An Example of a Nascent Continental Fold-and-Thrust Belt", *Journal Geophys. Res.*, **92**, 441-460.

18. Molnar, P. and Lyon-Caen, H. (1989). "Fault Plane Solutions of Earthquakes and Active Tectonics of Tibetan Plateau and Its Margin", *Geophys. Journal Int.*, **99**, 123-153.

19. Brune, J.N. (1970). "Tectonic Stress and the Spectra of Seismic Shear Waves from Earthquakes", *Journal Geophys. Res.*, **75**, 4997-5009.

20. Brune, J.N. (1971). "Correction (to Brune, 1970)", *Journal Geophys. Res.*, **76**, 5002.

21. Keilis-Borok, V.I. (1959). "On the Estimation of the Displacement in an Earthquake Source and Source Dimensions", Ann. Geofis., **12**, 205-214.

22. Madariaga, R. (1976). "Dynamics of the Expanding Circular Fault", Bull. Seismol. Soc. Am, **66**, 639-666.

23. Sato, T. and Hirasawa, T. (1973). "Body Wave Spectra from Propagating Shear Cracks", *Journal Physics of the Earth*, **21**, 415-431.

24. Bresnev, A. (2002). "Source Parameters Observable from Corner Frequency of Earthquake Spectra", Bulletin of the Seismological Society of America, **92**(5), 2047-2048.

25. Hanks, T.C. and Wyss, M. (1972). "The Use of Body-Wave Spectra in the Determination of Seismic-Source Parameters", Bull. Seismol. Soc. Am., **62**, 561-589.

26. Aki, K. (1966). "Generation and Propagation of

G-Waves from the Niigata Earthquake of June 16, 1964. Part 2. Estimation of Earthquake Moment, Released Energy, and Stress-Strain Drop from the G-Waves Spectrum", Bull. Earthquake Res. Ins., Tokyo Univ., **44**, 73-88.

27. Archuleta, R.J., Cranswinck, E., Mueller, CH., and Spudich., P. (1982). "Source Parameters of the 1980 Mammoth Lakes, California, Earthquake Sequence", *Journal Geophys. Res.*, **87**, 4595-4607.